THE JOURNAL OF BIOLOGICAL CHEMISTRY VOL. 288, NO. 25, pp. 18260–18270, June 21, 2013

Structural and Biochemical Characterization of Compounds Inhibiting *Mycobacterium tuberculosis* Pantothenate Kinase*

Received for publication, April 11, 2013, and in revised form, May 7, 2013 Published, JBC Papers in Press, May 9, 2013, DOI 10.1074/jbc.M113.476473

Christofer Björkelid[‡1], Terese Bergfors[‡], Anand Kumar V. Raichurkar[§], Kakoli Mukherjee[§], Krishnan Malolanarasimhan[§], Balachandra Bandodkar[§], and T. Alwyn Jones[‡]

From the [‡]Department of Cell and Molecular Biology, Uppsala University, Biomedical Center, SE-751 24 Uppsala, Sweden and [§]AstraZeneca India Private, Ltd., Bellary Road, Hebbal, Bangalore 560024, India

Background: Pantothenate kinase (PanK), an essential enzyme for *Mycobacterium tuberculosis*, catalyzes the rate-limiting step in the CoA pathway.
Results: Structures of *M. tuberculosis* PanK, complexed with new inhibitors, were determined, and their inhibitions were evaluated biochemically.
Conclusion: Inhibitor binding overlaps with the substrate/product sites; also, an alternative mode of ATP binding is proposed.
Significance: These are the first structures of a type I PanK complexed with inhibitors.

***Mycobacterium tuberculosis*, the bacterial causative agent of tuberculosis, currently affects millions of people. The emergence of drug-resistant strains makes development of new antibiotics targeting the bacterium a global health priority. Pantothenate kinase, a key enzyme in the universal biosynthesis of the essential cofactor CoA, was targeted in this study to find new tuberculosis drugs. The biochemical characterizations of two new classes of compounds that inhibit pantothenate kinase from *M. tuberculosis* are described, along with crystal structures of their enzyme-inhibitor complexes. These represent the first crystal structures of this enzyme with engineered inhibitors. Both classes of compounds bind in the active site of the enzyme, overlapping with the binding sites of the natural substrate and product, pantothenate and phosphopantothenate, respectively. One class of compounds also interferes with binding of the cofactor ATP. The complexes were crystallized in two crystal forms, one of which is in a new space group for this enzyme and diffracts to the highest resolution reported for any pantothenate kinase structure. These two crystal forms allowed, for the first time, modeling of the cofactor-binding loop in both open and closed conformations. The structures also show a binding mode of ATP different from that previously reported for the *M. tuberculosis* enzyme but similar to that in the pantothenate kinases of other organisms.**

Pantothenate kinase (PanK,[2] EC 2.7.1.33) catalyzes the first and rate-limiting step in the universal CoA biosynthetic pathway, where pantothenate (vitamin B_5) is converted to 4′-phosphopantothenate using ATP as a cofactor (1). Three types of PanK have been described, which differ in their biochemical and structural characteristics. Type I, encoded by the gene *coaA* (2), is found in a large number of bacterial species and is tightly feedback-regulated by CoA and its thioesters (3). It is exemplified by the extensively studied *Escherichia coli* PanK (*Ec*PanK; Ref. 4, 5). The type II enzyme is mostly found in eukaryotes. Humans express four isoforms of the enzyme, named PanK1 to 4. Defects in the *panK2* gene have been linked to neurodegenerative disease (6, 7). Based on sequence and structural homology some bacterial enzymes, such as *Staphylococcus aureus* PanK, are also classified as type II enzymes. Whereas the eukaryotic PanKs are feedback-regulated by CoA, the *S. aureus* enzyme is not (8). Type III, encoded by the gene *coaX*, is the most widespread type of the enzyme, with homologs present in 12 of the 13 major bacterial groups (9). It is not inhibited by CoA or its thioesters (10). Many bacteria have two PanK genes coding for different types of the enzyme.

Tuberculosis, caused by the pathogenic bacterium *Mycobacterium tuberculosis*, is estimated to infect one-third of the world population and is responsible for ~1.4 million deaths annually (World Health Organization, 2011). High-burden countries for tuberculosis are found in sub-Saharan Africa, with high rates of the deadly combination of HIV and tuberculosis. Current treatment of tuberculosis relies on the frontline drugs isoniazid and rifampicin, developed in the 1950s and 1960s. Increasing incidence rates of multidrug-resistant tuberculosis, resistant to front-line drugs, and extensively drug-resistant tuberculosis, resistant to front-line and second-line drugs, make development of new antibiotics targeting *M. tuberculosis* a global health priority.

The *M. tuberculosis* genome contains both *coaA* and *coaX* genes, coding for a type I and type III PanK, respectively. However, it has been shown that *coaA* is the only PanK gene essential for bacterial growth *in vitro* and *in vivo* (11). The *M. tuberculosis* type I PanK (*Mt*PanK) is a 312-amino acid (36 kDa) P-loop kinase with a central seven-stranded β-sheet surrounded by α-helices, containing a Walker A motif for nucleo-

* This work was supported by the Foundation for Strategic Research, the Swedish Research Council, and Uppsala University.
The atomic coordinates and structure factors (codes 4BFS, 4BFT, 4BFU, 4BFV, 4BFW, 4BFX, 4BFY, and 4BFZ) have been deposited in the Protein Data Bank (http://wwpdb.org/).
[1] To whom correspondence should be addressed: Dept. of Cell and Molecular Biology, Uppsala University, Biomedical Ctr., Box 596, SE-751 24 Uppsala, Sweden. Tel.: 46-18-471-4982; Fax: 46-18-530396; E-mail: christofer@xray.bmc.uu.se.
[2] The abbreviations used are: PanK, pantothenate kinase; *Mt*PanK, *M. tuberculosis* type I PanK; *Ec*PanK, *E. coli* PanK; PDB, Protein Data Bank; r.m.s.d., root mean square deviation; *Cb*PanK, *Coxiella burnetii* PanK.

tide binding (12). It functions as a homodimer. *Mt*PanK has been the target for extensive structural studies and has been crystallized in complex with its substrates, products, adenosine or guanosine cofactors, and feedback inhibitor CoA (13–16). The *Mt*PanK structures in this study represent the first complexes with engineered inhibitory compounds and provide a starting point for development of novel antibiotics targeting pathogens that are dependent on type I PanK.

EXPERIMENTAL PROCEDURES

Protein Expression and Purification—The gene encoding *Mt*PanK (*coaA*, Rv1092c) was PCR-amplified from genomic DNA, and an N-terminal His_6 tag was added. The resulting construct was ligated into a pET15b expression vector (Novagen) using restriction enzymes NdeI and BamHI. Correct ligation of the sequence coding for a full-length His-tagged *Mt*PanK was confirmed by sequencing. The resulting expression vector was used to transform *E. coli* BL21-AI competent cells (Invitrogen). Cells were incubated at 37 °C in Luria-Bertani growth medium, with 100 μg/ml ampicillin. Expression was induced by adding 0.2% (w/v) L-arabinose, at $A_{600} \approx 0.6$, and cells were further incubated at 37 °C for 3 h. Cells were centrifuged at 4500 × *g* for 30 min, and the resulting cell pellet was resuspended in lysis buffer (50 mM Tris-HCl, pH 8.0, 300 mM NaCl, 20 mM imidazole) with 0.01 mg/ml RNase and 0.02 mg/ml DNase. Cells were lysed in a cell disruptor (Constant Systems, Ltd.) and the lysate was centrifuged at 18,000 × *g* for 30 min to remove cell debris. The His-tagged protein was then purified by binding it on a nickel-Sepharose (GE Healthcare) column. The column was washed with 10 column volumes of wash buffer (50 mM Tris-HCl, pH 8.0, 300 mM NaCl, 50 mM imidazole), and the protein was eluted with 4 column volumes of elution buffer (50 mM Tris-HCl, pH 8.0, 300 mM NaCl, and 500 mM imidazole). The elution fractions were pooled and then diluted at a 2:1 ratio with gel filtration buffer (50 mM Hepes, pH 7.5, 300 mM NaCl, 2% (v/v) glycerol, and 10 mM β-mercaptoethanol). The diluted protein sample was further purified using a Superdex 75 (GE Healthcare) size-exclusion column, pre-equilibrated with gel filtration buffer. A modified gel filtration buffer (50 mM Tris-HCl, pH 7.5, 300 mM NaCl, 10% (v/v) glycerol, 2 mM DTT, and 0.1 mM EDTA) was used in subsequent purifications of the enzyme for biochemical studies. Elution fractions were pooled, and analysis by SDS-PAGE showed it to contain ~99% pure protein of correct size. Protein aliquots were stored at −70 °C. Only once-thawed aliquots were used for each experiment.

IC_{50}, Minimum Inhibitory Concentration , and Thermal Stability Measurements—The biochemical and thermal shift assays have been described in detail by Venkatraman *et al.* (17). Briefly, *Mt*PanK activity was measured in a pyruvate kinase-lactate dehydrogenase-coupled assay where the reaction rate was determined by spectrophotometric measurement of NADH consumption. IC_{50} measurements were performed with a suitable concentration range of inhibitory compound, while keeping the concentration of pantothenate and ATP at 122 and 395 μM, respectively, which is their respective K_m (17). A second set of IC_{50} measurements were performed with the ATP concentration at 50× K_m, to determine the effect of cofactor competition.

Thermal stability measurements were recorded with a real-time PCR thermal cycler where the fluorescence of SYPRO orange dye (Invitrogen) was used to monitor protein unfolding in the absence or presence of 25 μM inhibitory compound, at temperature intervals of 0.5 °C, from 25 °C to 85 °C. Measurements were repeated with the addition of 0.5 and 1.0 mM ATP.

The minimum inhibitory concentration assay was set up as per the Clinical and Laboratory Standards Institute guidelines. These assays were done in 96-well plate format, and the readout was by Microplate Alamar Blue Assay (18).

Crystallization—The purified protein was concentrated to 12 mg/ml in 20 mM Tris-HCl, pH 8.0, 0.3 M NaCl, 10 mM β-mercaptoethanol, and 10% (v/v) glycerol for initial crystallization trials. Trials were set up with the sitting-drop vapor diffusion method on an Oryx 6 robot (Douglas Instruments) in two-well MRC plates (Molecular Dimensions). Droplets composed of 0.3 μl of protein solution and 0.3 μl of reservoir solution were equilibrated against 80 μl of the latter. Inhibitors were dissolved in dimethyl sulfoxide. For cocrystallization experiments, a 10-molar excess of the inhibitor with and without 5 mM ATP and 1 mM $MgCl_2$ was added to the protein immediately before crystallization trials. In addition, five non-hydrolyzable ATP analogues (Jena Bioscience, catalog no. NK-101), adenosine, adenosine ribose, and ADP were substituted for ATP.

Crystals of a binary complex (*Mt*PanK-**1a**) in space group $P3_121$ grew in 3–4 days at 20 °C from condition E11 of the JCSG+ screen (Qiagen) containing 14.4% (w/v) PEG 8000, 20% (v/v) glycerol, 0.08 M sodium cacodylate, pH 6.5, and 0.16 M calcium acetate. The optimized crystallization conditions were essentially the same except that magnesium chloride replaced the calcium. The cryosolution for these crystals consisted of 35% (w/v) PEG 3350, 0.2 M cacodylate, 10 mM $MgCl_2$, and, where appropriate, 1 mM inhibitor. Crystals were placed in the cryosolution for 5 s before vitrification in liquid nitrogen. Soaking experiments on apo-crystals with this space group were unsuccessful.

Crystals of seven different ternary complexes (*Mt*PanK-inhibitor-PO_4) in space group $P2_12_12$ were obtained with 1.8 M sodium/potassium phosphate, pH 8.2 (Quik screen, Hampton Research) at 20 °C in a 3–4 days. For optimization of these crystals, the protein concentration was reduced to 5 mg/ml, and the drops were seeded. These drops (0.5 μl each of protein and reservoir solution) were set up manually and equilibrated against 1 ml of the reservoir solution (1.8 M sodium/potassium phosphate, pH 8.2) in Nextal 24-well plates (Qiagen). The ternary complexes were obtained either by cocrystallization or soaking. The crystals (0.1 × 0.2 × 0.2 mm) were vitrified directly from the drops.

Data Collection and Processing—Diffraction data from *Mt*PanK, co-crystallized or soaked with inhibitors, were collected from single crystals at the European Synchrotron Radiation Facility (Grenoble, France) or MAXlab (Lund, Sweden). Diffraction data were indexed and integrated using MOSFLM (19) and scaled with SCALA (20). These programs are part of the CCP4 program package (21). Data collection statistics are shown in Table 1.

Structure Determination and Refinement—The *Mt*PanK-**1a** binary complex (see Table 1) was crystallized in space group $P3_121$, isomorphous with the published *Mt*PanK-CoA structure (PDB code 2GEV; Ref. 13). These coordinates were stripped of ligands and water molecules and subjected to an initial round of rigid body crystallographic refinement with REFMAC5 (22). The seven structures of the *Mt*PanK-inhibitor-PO_4 ternary complexes (see Table 1) in space group $P2_12_12$ were solved by molecular replacement with the program PHASER (23), using the refined *Mt*PanK-**1a** structure, stripped of ligands and waters, as a search model.

All eight structures were improved by multiple, alternating cycles of crystallographic refinement with REFMAC5 and interactive rebuilding using the program *O* (24). Waters were added using the carbonyl oxygen profiling methods implemented in *O*. Coordinates and stereochemical restraints for inhibitory compounds were generated in *O*, and stereochemical dictionaries for refinement were generated by REFMAC5. Refinement statistics are shown in Table 1.

Other Methods—Structural figures were created in *O* and rendered with MOLRAY (25). Detailed structural comparisons were made in *O* with Cα matching pair cutoffs of 3.8 Å (26). Sequence alignments were made using ClustalW (27), and the corresponding figure was designed with ALINE (28).

RESULTS

Sequence Alignment—The sequence alignment of type I PanK sequences from 13 pathogenic bacterial species shows that the sequences are highly conserved, with a minimum of 41% pairwise sequence conservation (Fig. 1). The longest stretches of conserved residues are found around the P-loop, where the Walker A motif is identical in all 13 species, as are residues involved in substrate and cofactor binding. The *Mt* enzyme differs from the rest in the loop formed by residues 79–91 (*Mt*PanK numbering), flanked by helix α4 and strand β2, which is extended by four residues. Some variation is seen in the length of the loop formed by residues 203–213 (*Mt*PanK numbering), flanked by strand β6 and helix α10.

*The MtPanK-**1a** Binary Complex*—The *Mt*PanK-**1a** binary complex was solved in space group $P3_121$, with one molecule in the asymmetric unit, and refined to a crystallographic R factor of 19.9% at a resolution of 2.9 Å (see Table 1 for crystallographic data). The crystal structure is in the same space group and has similar unit cell parameters as the previously reported *Mt*PanK structures. It is isomorphous to what has been called crystal form II of the enzyme (13). The *Mt*PanK-**1a** structure can be superimposed on all previously described *Mt*PanK structures with root mean square deviations (r.m.s.d.) from 0.3 to 0.6 Å for 302 paired Cα atoms. The greatest differences between the *Mt*PanK structures in this space group are located at the N-terminal and the loop formed by residues 79–91, which adopt different conformations in crystal forms I and II of the enzyme (13). The flexible part of this loop, residues 81–87, is disordered in our *Mt*PanK-**1a** structure and has therefore been omitted from the model as well as the disordered first five residues and the N-terminal His tag.

The MtPanK-inhibitor-PO_4 Ternary Complexes—Structures of seven ternary complexes of *Mt*PanK with inhibitory compounds and phosphate ions were solved in space group $P2_12_12$ (see Table 1 for crystallographic data). This is a new space group for this enzyme. One of these complexes, the *Mt*PanK-**2b**-PO_4 complex, diffracts to a resolution of 2.1 Å, which is the highest resolution reported for a type I PanK crystal structure. The structures in this space group have a complete homodimer in the asymmetric unit. This dimer is positioned such that the crystallographic 2-fold operator forms a tetramer with 222 point group symmetry. The active sites in both molecules contain a bound inhibitor and a phosphate ion. The first six residues and the N-terminal His tag are disordered in these structures and therefore omitted from the model. The A and B molecules of the homodimers can be superimposed with r.m.s.d. values ranging from 0.4 to 0.8 Å for all paired Cα atoms. The *Mt*PanK-**1a** binary complex, as a representative of the structures in the trigonal space group, can be superimposed on the *Mt*PanK-inhibitor-PO_4 ternary complexes with an average r.m.s.d. of 1.1 Å for both A and B molecules, for all paired Cα atoms. The main differences are found in the second half of helix α4 at the dimerization interface. Here the end point, Leu-78, is shifted ~6.5 Å as a result of helix bending, adopting a local conformation identical to that of the *Ec*PanK (5, 29) and *Coxiella burnetii* PanK (*Cb*PanK)[3] structures (Fig. 2). Another difference is the cofactor-binding loop, or adenosine lid, which adopts an open conformation, in contrast to the closed conformation seen in all previous *Mt*PanK structures (discussed in detail below). The open conformation of this loop forces a shift of helix α1 and the loop between helices α1 and α2.

The *Mt*PanK-inhibitor-PO_4 ternary complex dimers superimpose on the various *Ec*PanK or *Cb*PanK dimers with average r.m.s.d. values of 1.3 and 1.2 Å, respectively, with more than ~570 paired Cα atoms. Although the structures of the central β-sheet and the P-loop are highly conserved in all PanK structures, differences can be seen in the surrounding helices and loops. The main differences between the *Mt*-, *Ec*-, and *Cb*PanKs are located to the loop formed by residues 203–213 (*Mt*PanK numbering), flanked by strand β6 and helix α10 (Fig. 1). This loop is elongated by seven residues in the *Ec* and *Cb* enzymes and extends away from the center of the molecule in different conformations (Fig. 2). However, the loop formed by residues 79–91 (*Mt*PanK numbering), flanked by helix α4 and strand β2, is elongated by four residues in the *Mt* enzyme (Figs. 1 and 2).

Binding of Inhibitors—We have determined crystal structures of eight protein-inhibitor complexes of *Mt*PanK with inhibitors of two different classes. Compounds **1a** to **1f** are triazoles, whereas compounds **2a** and **2b** are biaryls (Table 2). Electron density is well defined for all of these inhibitors, except for the slightly less well defined electron density of the difluorophenyl ring in **1f** (Fig. 3).

The binding mode of the triazole compounds is exemplified by triazole **1a** in Fig. 4*a*. They overlap with pantothenate (*Mt*PanK-Pan-AMPPCP, PDB code 2ZSE; Ref. 14), and the

[3] M. C. Franklin, J. Cheung, M. Rudolph, M. Cassidy, E. Gary, F. Burshteyn, and J. Love, unpublished work.

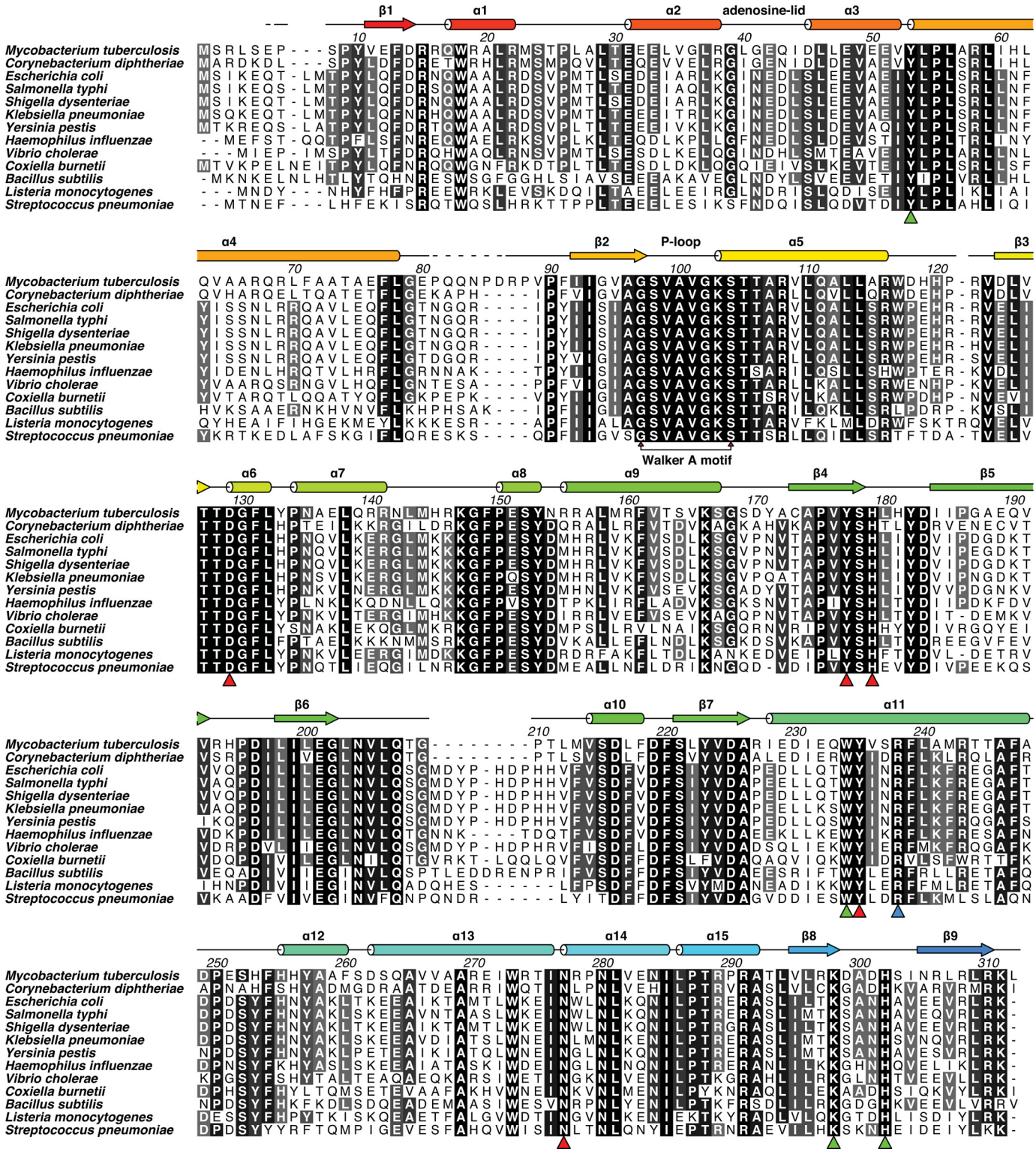

FIGURE 1. **Sequence alignment of type I PanKs from various pathogenic bacteria.** *Mt*PanK numbering and secondary structure are shown as defined by Das *et al.* (13). The *blue triangle* shows residue Arg-238, interacting with the phosphate bound in the P-loop, or inhibitory compounds. *Red triangles* show residues involved in pantothenate/phosphopantothenate binding. *Green triangles* show residues involved in adenine binding in the nucleoside binding site reported for *Ec*- and *Cb*PanK. Sequences used in this alignment were as follows: *Mt*PanK (UniProt ID P63810), *Corynebacterium diphtheriae* PanK (UniProt ID Q6NI48), *Ec*PanK (UniProt ID P0A6I3), *Salmonella typhi* PanK (UniProt ID Q8Z318), *Shigella dysenteriae* PanK (UniProt ID Q32aF0), *Klebsiella pneumoniae* PanK (UniProt ID G0GSU7), *Yersinia pestis* PanK (UniProt ID Q8ZAN6), *Haemophilus influenzae* PanK (UniProt ID P44793), *Vibrio cholerae* PanK (UniProt ID Q9KV38), *Coxiella burnetii* PanK (UniProt ID Q83EV9), *Bacillus subtilis* PanK (UniProt ID P54556), *Listeria monocytogenes* PanK (UniProt ID Q8Y8I0), and *Streptococcus pneumoniae* PanK (UniProt ID Q97RH6).

TABLE 1
Data collection and refinement statistics

	*Mt*PanK-1a	*Mt*PanK-1b-PO_4	*Mt*PanK-1c-PO_4	*Mt*PanK-1d-PO_4	*Mt*PanK-1e-PO_4	*Mt*PanK-1f-PO_4	*Mt*PanK-2a-PO_4	*Mt*PanK-2b-PO_4
Data collection								
PDB code	4BFS	4BFT	4BFU	4BFV	4BFW	4BFX	4BFY	4BFZ
Beam line	I911-2, MAXlab	ID14-1, ESRF[a]	ID14-4, ESRF	ID14-1, ESRF	ID23-1, ESRF	ID14-4, ESRF	ID14-1, ESRF	ID14-4, ESRF
Detector	MAR 165	ADSC Q210	ADSC Q315r	ADSC Q210	ADSC Q315r	ADSC Q315r	ADSC Q210	ADSC Q315r
Wavelength (Å)	1.0412	0.9340	0.9795	0.9334	1.0723	0.9795	0.9334	0.9795
Space group	$P3_121$	$P2_12_12$	$P2_12_12$	$P2_12_12$	$P2_12_12$	$P2_12_12$	$P2_12_12$	$P2_12_12$
Cell axial lengths (Å)	105.28, 105.28, 90.80	88.40, 149.69, 62.77	88.60, 150.69, 63.18	88.33, 151.77, 63.13	89.03, 150.71, 60.50	88.01, 149.51, 62.83	88.29, 149.28, 61.91	88.46, 148.28, 63.26
V_m ($Å^3$/Da)[b]	4.07	2.91	2.96	2.97	2.85	2.90	2.86	2.91
Resolution range (Å)[c]	30.0–2.90 (3.06–2.90)	40.0–2.29 (2.41–2.29)	60.0–2.28 (2.40–2.28)	40.0–2.29 (2.42–2.29)	50.0–2.27 (2.39–2.27)	60.0–2.70 (2.85–2.70)	44.0–2.30 (2.42–2.30)	58.0–2.10 (2.21–2.10)
No. of reflections measured	78,322 (11,264)	136,311 (19,054)	266,498 (38,455)	280,048 (40,356)	125,447 (18,679)	148,478 (21,019)	168,008 (22,704)	341,894 (50,728)
No. of unique reflections	13,018 (1865)	37,958 (5478)	39,320 (5655)	38,852 (5589)	38,286 (5516)	23,491 (3392)	34,705 (4857)	49,393 (7134)
Average multiplicity	6.0 (6.0)	3.6 (3.5)	6.8 (6.8)	7.2 (7.2)	3.3 (3.4)	6.3 (6.2)	4.8 (4.7)	6.9 (7.1)
Completeness (%)	98.9 (99.5)	99.4 (99.3)	99.3 (99.3)	100 (100)	99.6 (99.7)	99.9 (99.9)	93.6 (91.6)	99.9 (100.0)
R_{merge}[d,e]	0.115 (0.491)	0.111 (0.486)	0.085 (0.430)	0.095 (0.399)	0.102 (0.500)	0.114 (0.495)	0.106 (0.431)	0.107 (0.491)
R_{meas}[f]	0.127 (0.537)	0.130 (0.571)	0.093 (0.466)	0.103 (0.430)	0.122 (0.593)	0.124 (0.541)	0.118 (0.483)	0.116 (0.529)
$R_{p.i.m.}$[g]	0.051 (0.213)	0.066 (0.291)	0.036 (0.176)	0.038 (0.159)	0.066 (0.316)	0.049 (0.215)	0.051 (0.209)	0.044 (0.197)
$\langle I/\sigma I \rangle$	10.1 (3.3)	10.1 (2.6)	12.3 (3.7)	19.2 (5.0)	6.9 (2.3)	10.6 (3.4)	9.3 (3.2)	12.0 (3.9)
Refinement statistics								
Resolution range (Å)	30.0–2.90 (2.98–2.90)	40.0–2.29 (2.35–2.29)	60.0–2.28 (2.33–2.28)	40.0–2.29 (2.35–2.29)	50.0–2.27 (2.33–2.27)	60.0–2.70 (2.77–2.70)	44.0–2.30 (2.36–2.30)	58.0–2.10 (2.16–2.10)
No. of reflections used in working set	12,375 (807)	36,047 (2420)	37,299 (2497)	36,854 (2466)	36,326 (2446)	22,238 (1455)	32,917 (2166)	46,841 (3162)
No. of reflections for R_{free} calculation	639 (41)	1905 (125)	1972 (135)	1946 (138)	1912 (135)	1208 (82)	1747 (105)	2501 (170)
R (%)[c]	19.9	22.5	22.1	20.6	21.6	20.9	20.3	20.7
R_{free} (%)	24.5	28.6	26.3	26.2	27.3	28.5	25.7	24.8
No. of non-hydrogen atoms	2484	5109	5148	5229	5164	5075	5226	5307
No. of solvent waters	13	99	136	213	134	63	210	289
Average *B*-factors ($Å^2$)								
Protein atoms (A, B)	52.0, −[h]	45.4, 43.1	47.3, 48.8	32.0, 32.1	42.7, 46.3	44.6, 45.6	30.6, 33.9	30.5, 31.9
Solvent atoms	34.7	34.4	41.9	29.2	38.7	33.5	30.0	32.1
Inhibitory compound (A, B)	73.7, −	51.6, 40.0	47.2, 51.3	34.9, 34.0	47.9, 50.5	64.8, 71.4	21.1, 24.4	22.8, 24.4
Phosphate ion (A, B)	−	31.5, 33.8	36.5, 34.9	22.2, 26.2	29.3, 31.3	37.5, 37.9	21.7, 24.9	26.4, 24.9
Ramachandran plot outliers (A, B) (%)[i]	3.5, −	5.2, 5.5	6.5, 3.1	5.2, 4.1	4.1, 7.2	4.1, 4,5	3.8, 5.5	3.1, 2.7
r.m.s.d. from ideal bond length (Å)[j]	0.009	0.012	0.011	0.010	0.012	0.009	0.011	0.009
r.m.s.d. from ideal bond angle	1.479°	1.795°	1.650°	1.612°	1.897°	1.564°	1.725°	1.501°

[a] ESRF indicates the European Synchrotron Radiation Facility.
[b] Values were calculated using methods described by Matthews (Ref. 31).
[c] Values in parentheses refer to the outer resolution shell.
[d] Merging and crystallographic *R*-factors were generated by the computer programs described under "Experimental Procedures."
[e] $R_{merge} = \Sigma_{hkl}\Sigma_i|I_i(hkl) - \langle I(hkl)\rangle|/\Sigma_{hkl}\Sigma_i I_i(hkl)$.
[f] $R_{meas} = \Sigma_{hkl}[N/(N-1)]^{1/2}\Sigma_i|I_i(hkl) - \langle I(hkl)\rangle|/\Sigma_{hkl}\Sigma_i I_i(hkl)$.
[g] $R_{p.i.m.} = \Sigma_{hkl}[1/(N-1)]^{1/2}\Sigma_i|I_i(hkl) - \langle I(hkl)\rangle|/\Sigma_{hkl}\Sigma_i I_i(hkl)$.
[h] −, value is not applicable.
[i] Calculated using a strict boundary Ramachandran plot definition (Ref. 32).
[j] Ideal values are from Engh & Huber (Ref. 33).

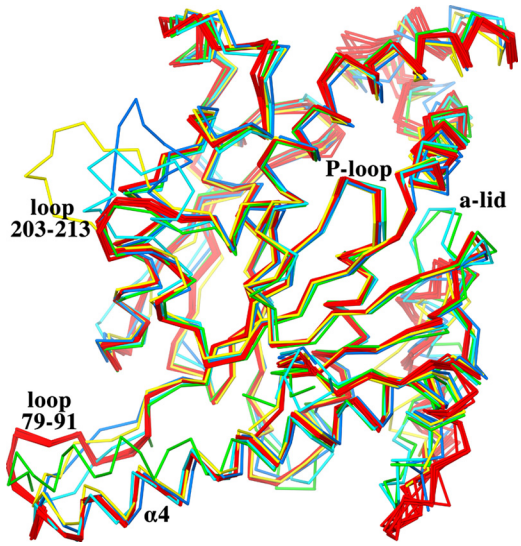

FIGURE 2. **Cα superposition of A molecules of all *Mt*PanK-inhibitor-PO_4 complexes (*red*), *Mt*PanK-1a (*green*), *Ec*PanK-CoA (*light blue*, PDB code 1ESM), *Ec*PanK-Pan-ADP (*blue*, PDB code 1SQ5), and *Cb*PanK-ADP (*yellow*, PDB code 3TQC).** Shown is the conserved conformation of the P-loop, the open and closed form of the adenosine lid (*a-lid*), the alternative conformation of helix α4, and the two loops (with *Mt*PanK numbering) elongated in *Mt*PanK, *Ec*PanK, or *Cb*PanK.

pantothenate moieties of phosphopantothenate (*Mt*PanK-PPan-ADP, PDB code 2ZSA; Ref. 14) and CoA (*Mt*PanK-CoA, PDB code 2ZSD) in the active site pocket (Fig. 5, *a* and *b*, respectively). These compounds fan out from the conserved triazole ring to form similar U-shaped conformations where the halogen-substituted phenyl rings are roughly co-planar, with ring edges abutting. In the **1b** complex, for example, the vector normals to the phenyl rings form a 51° angle, with ring centers separated by 7.8 Å, and the pair of ring edge carbons separated by ~5.5–6.5 Å. Each triazole ring forms a pair of conserved hydrogen bond interactions with side chains that are themselves highly conserved (Fig. 4*a*). Residues Tyr-235 and Asn-277 are involved in pantothenate and phosphopantothenate binding (14), respectively, but here, the hydroxyl group of Tyr-235 forms a hydrogen bond to one nitrogen in the triazole ring, whereas the amide group of the side chain of Asn-277 hydrogen bonds to another (Fig. 4*a*). Hydrogen bonding atoms in the peptide linkage make interactions with water molecules, where visible, except in the **1c** complex where the carbonyl oxygen directly interacts with the hydroxyl of Tyr-177. No hydrogen bonding interactions are observed to the ether-linking oxygen. The removal of the ether-linked oxygen in **1c** is easily accommodated by the inhibitor. Here, we see a ~0.7 Å shift in the fluorophenyl group. This involves a small pivot of the triazole

TABLE 2

Structures of the inhibitory compounds and results from the biochemical assay, thermal shift, and MIC measurements

ND, not determined.

Structure	Class	Compound ID	IC_{50} at K_m for ATP (μM)	IC_{50} at 50x K_m for ATP (μM)	*Mt* MIC (μg/ml)	Tm shift with 0.0 mM ATP (°C)	Tm shift with 0.5 mM ATP (°C)	Tm shift with 1.0 mM ATP (°C)	Mode of Inhibition
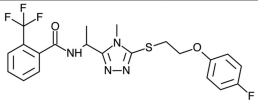	Triazole	**1a**	0.09	5.5	>64	3.8	1.1	0.9	Competitive
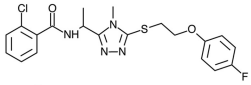	Triazole	**1b**	1.13	>12.5	>64	1.8	0.4	0.3	Competitive
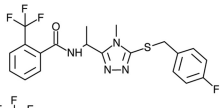	Triazole	**1c**	0.15	10.36	>64	3.7	1.8	0.4	Competitive
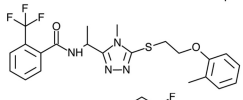	Triazole	**1d**	0.14	2.82	>32	3.9	1.7	1.8	Competitive
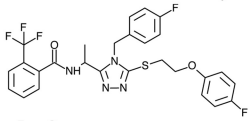	Triazole	**1e**	0.05	0.69	>32	4.6	2.5	2.9	Competitive
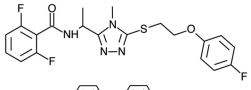	Triazole	**1f**	1.09	14.0	>64	2.4	1.0	0.7	Competitive
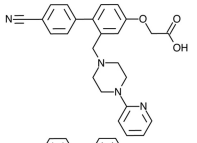	Biaryl	**2a**	0.12	0.13	>64	2.4	4.8	4.6	Non-competitive
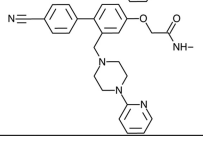	Biaryl	**2b**	0.55	ND	>64	ND	ND	ND	Non-competitive

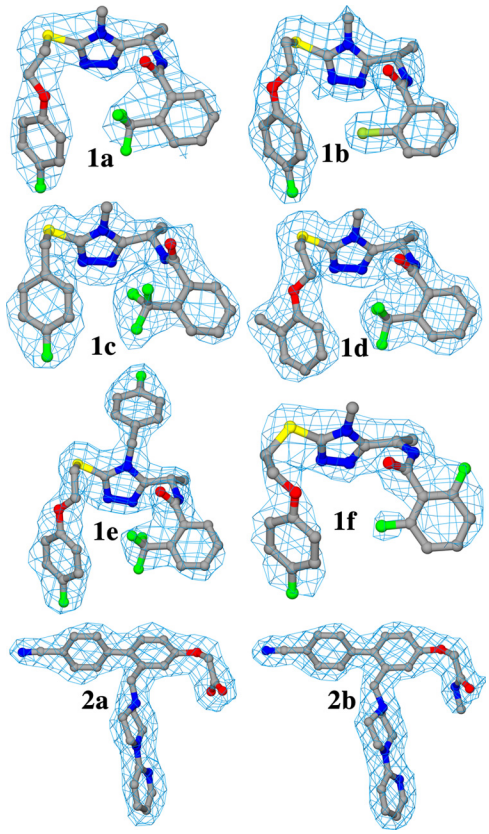

FIGURE 3. **Representative electron density for inhibitors in the A molecules of their respective complex structure.** The σA-weighted ($2m|F_o| - D|F_c|$) electron density maps (34) are drawn at the level of the root mean square value of the respective map.

ring that maintains the protein-inhibitor hydrogen bonds but results in relatively large local changes in the enzyme. In particular, the side chain of Tyr-182 takes on a different rotamer conformation compared with all the other complexes. The tyrosyl ring comes closer to the space vacated by the truncated ether linkage, and there is a rigid-body shift in helix α12, one of the helices that define the binding site. A much larger change in structure has been made in **1e** where a *para*-fluorobenzyl ring extends from the triazole ring. This change is easily accommodated by the enzyme, fitting into a preformed hydrophobic tunnel in the active site whose surface is created from four segments of the enzyme (helix α12 and α13, the loop between helix α7-α8 and sheets β4–β5).

Many of the fluorine atoms are involved in the electrostatic interactions described by Müller *et al.* (30). One of the phenyl rings has a *para*-fluorine atom in five of the six triazole compounds, and this ring binds in a mostly hydrophobic pocket made up of side chains Val-99, Ala-100, Tyr-235, Phe-239, and Met-242. The side chain of Arg-238, however, stretches to the bound phosphate in the orthorhombic crystal forms (for five of the six triazoles), to form a salt link. The *para*-fluorophenyl ring is approximately parallel to the plane of the guanidinium group with the fluorine atom ~3.3 Å above the plane. Another salt link exists between Asp-129 and His-179. The trifluoro-methyl at the *ortho*-phenyl substitution of **1e**, for example, is 3.3 Å from a nitrogen of the imidazole ring but is more distant in the **1c** complex (closest contact at 3.8 Å) as a consequence of the structural rearrangement in the enzyme. The relative orientation of the phenyl rings also means that the trifluoro-methyl group in one ring points toward the edge of the second ring in these structures.

The biaryl compounds, **2a** and **2b** (Fig. 4*b*), were both crystallized in ternary complexes with phosphate ions in the orthorhombic space group. These compounds also bind in the active site pocket, overlapping with the binding site of the triazole compounds (overlaid structure, Fig. 4*c*), and that of the pantothenate moieties in the previous *Mt*PanK structures (Fig. 5, *a* and *b*). In the **2b** complex, the Arg-238 side chain interacts with the phosphate ion as seen with the triazoles but changes conformation to form a salt link with the carboxylate of the inhibitor in the **2a** complex. The Tyr-182 side chain has the same rotamer conformation observed in the **1c** complex such that the hydroxyl group interacts with the ether linkage oxygen atom, as well as the carboxylate of one inhibitor and the amide nitrogen of the other (Fig. 4*b*). The *para*-nitrile phenyl group from each inhibitor packs into the hydrophobic tunnel used by the *para*-fluorobenzyl ring of **1e**. The conserved residues Tyr-235 and Asn-277 that are important for triazole binding do not interact directly with the biaryl class of compounds. Instead, they form hydrogen bonds to a water molecule that, in turn, interacts with a nitrogen of the piperazine ring. The 2-pyridyl nitrogen also forms a hydrogen bond to another water molecule, structurally equivalent to the water forming the same interaction with the peptide oxygen of the triazoles (Fig. 4*b*). When the triazole and biaryl complexes are superimposed on the ATP analogue complexes of *Ec*- and *Mt*PanK, the phosphate ion that we observe in the orthorhombic crystal form overlaps with the ATP β-phosphate group (Fig. 5*c*).

The Different Conformations of the Adenosine Lid—A structural feature of type I PanK enzymes is an adenosine-lid loop formed by residues 38–44 (*Mt*PanK numbering) and flanked by helices α2 and α3 (Figs. 1 and 2). The loop is in an open form when the adenosine moiety of ADP or ATP is bound, exemplified by the *Ec*PanK-Pan-ADP, *Ec*PanK-AMPPNP, and *Cb*PanK-ADP complex structures (Fig. 6*a*). In the absence of a bound adenosine, the loop adopts a closed conformation, exemplified by the *Ec*PanK-CoA structure (Fig. 6*b*). When switching from an open to closed conformation the loop shifts ~5 Å toward the adjacent helix α11. To accommodate this shift, the flanking helix α2 unwinds, contracting by one turn in the closed conformation. Helix α2 extends almost to helix α3 in the open form of the *Cb*Pank-ADP structure. The adenine ring of the cofactor is stacked between the loop and conserved residue His-302 (*Mt*PanK numbering), which in turn stacks with the ring of conserved residue Trp-234 (*Mt*PanK numbering) in the open form of the *Ec*PanK and *Cb*PanK structures (Fig. 6*a*). However, the *Mt*PanK structures crystallized in complex with nucleoside cofactors exhibit an alternative binding-mode (Fig. 5*c*; Refs. 15 and 16), where the adenine or guanine moieties occupy roughly the same binding site as the adenine moiety of CoA (Fig. 5*b*). In these structures, the adenosine lid retains a closed conformation, unable to accommodate a nucleoside in this binding site. In the *Mt*PanK-**1a** complex, crystallized in the previously reported trigonal space group, the adenosine lid

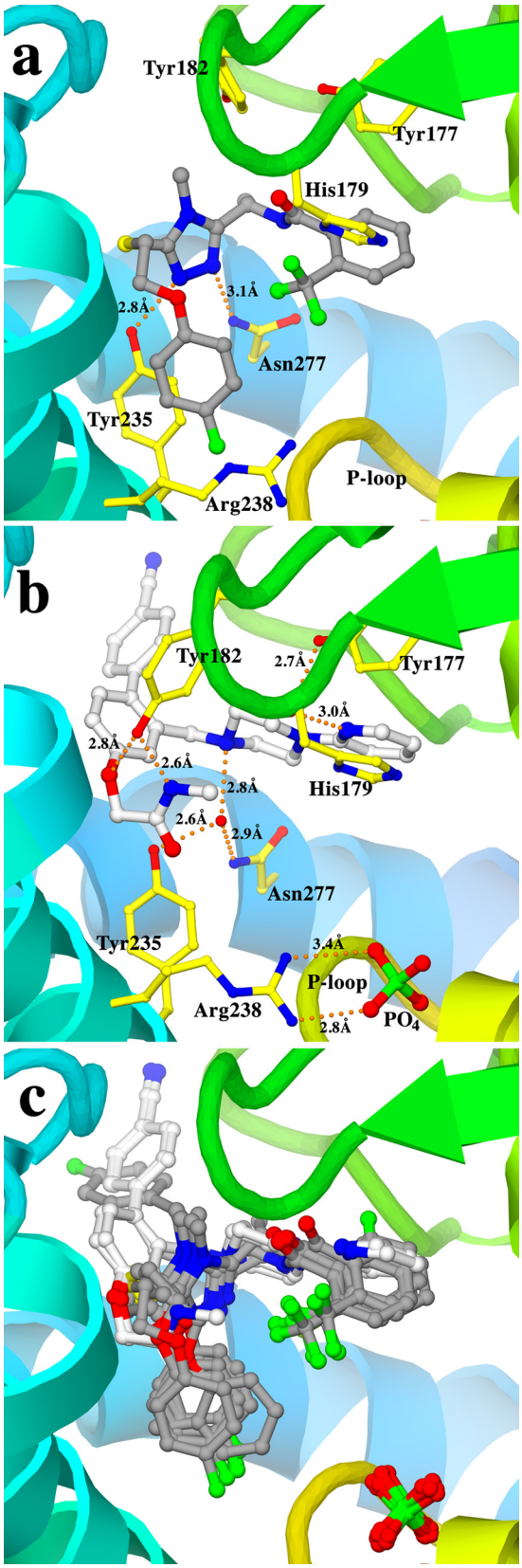

FIGURE 4. *a*, binding of a triazole compound (*gray* carbons) in the active site, exemplified by the *Mt*PanK-**1a** complex. Also shown are the residues involved in compound interactions and the P-loop. *b*, binding of a biaryl compound (*white* carbons) in the A molecule active site, exemplified by the *Mt*PanK-**2b**-PO_4 complex. Also shown are the residues involved in compound interactions (*yellow* carbons) and the phosphate ion bound in the P-loop. *c*, superposition of all triazole compounds (*gray* carbons) and biaryl compounds (*white* carbons) in the *Mt*PanK active site. The secondary structure is colored as in Fig. 1.

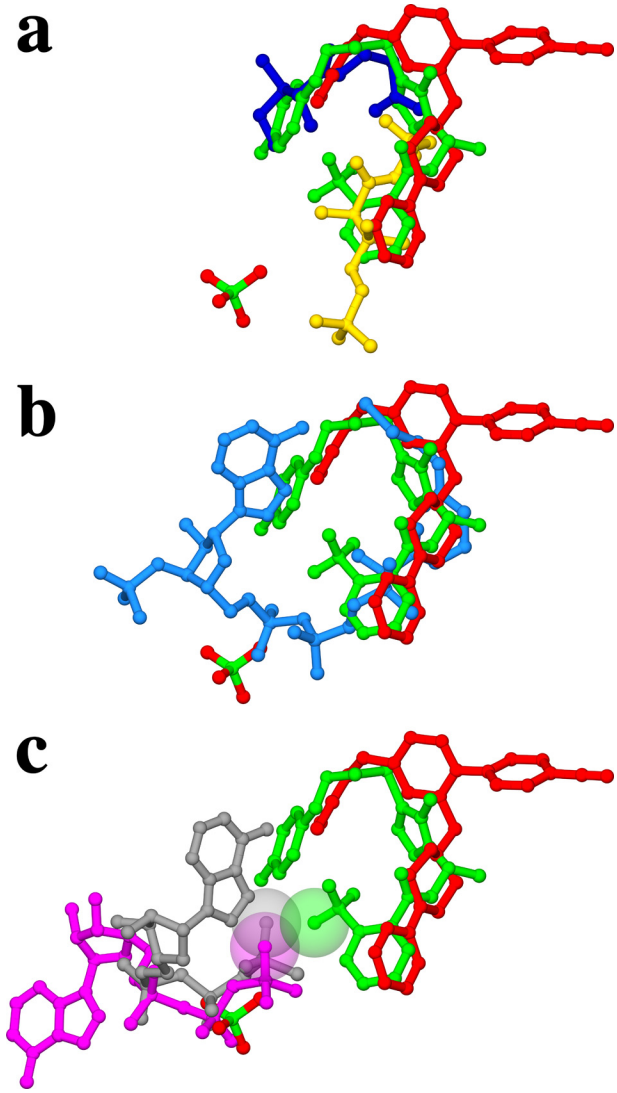

FIGURE 5. *a*, superposition of *Mt*PanK-**1a**, *Mt*PanK-**2b**-PO_4, *Mt*PanK-Pan-AMPPCP (PDB code 2ZSE) and *Mt*PanK-PPan-ADP (PDB code 2ZSA) showing the triazole compound **1a** (*green*), the biaryl-compound **2b** (*red*) with the phosphate ion (atom colors), pantothenate (*blue*), and phosphopantothenate (*yellow*). *b*, superposition of *Mt*PanK-**1a**, *Mt*PanK-**2b**-PO_4, and *Mt*PanK-CoA (PDB code 2ZSD) showing the triazole compound **1a** (*green*), the biaryl compound **2b** (*red*) with the phosphate ion (atom colors), and CoA (*light blue*). *c*, superposition of *Mt*PanK-**1a**, *Mt*PanK-**2b**-PO_4, *Mt*PanK-Pan-AMPPCP (PDB code 2ZSE) and *Ec*PanK-AMPPNP (PDB code 1ESN) showing the triazole compound **1a** (*green*), the biaryl compound **2b** (*red*) with the phosphate ion (atom colors), AMPPCP bound in the *Mt* structure (*gray*), and AMPPNP bound in the *Ec* structure (*magenta*). The van der Waals radii of the fluorine in compound **1a** and the γ-phosphate oxygen of AMPPCP and AMPPNP are shown as *transparent spheres*.

adopts a closed conformation, identical to all previously reported *Mt*PanK structures. However, in the *Mt*PanK-inhibitor-PO_4 structures crystallized in the orthorhombic space group, the loop adopts an open conformation. This conformation is similar to the open conformation of the *Ec*PanK and *Cb*PanK structures, although no adenosine is present in the adenosine-binding site (Fig. 6).

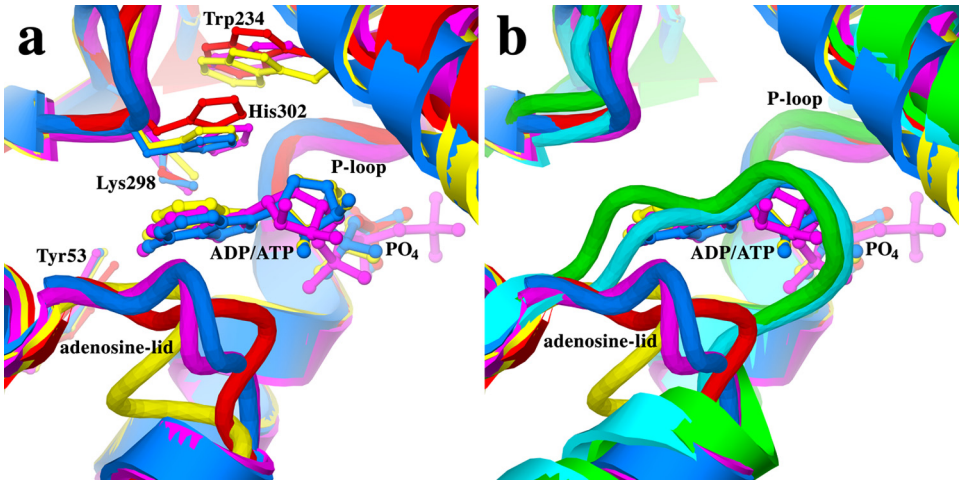

FIGURE 6. *a*, superposition of *Mt*PanK-**2b**-PO_4 (*red*), *Ec*PanK-AMPPNP (*magenta*, PDB code 1ESN), *Ec*PanK-Pan-ADP (*blue*, PDB code 1SQ5), and *Cb*PanK-ADP (*yellow*, PDB code 3TQC) showing the open form of the adenosine lid and conserved residues involved in adenosine binding. *b*, superposition of *Mt*PanK-**1a** (*green*), *Ec*PanK-CoA (*light blue*, PDB code 1ESM), *Mt*PanK-**2b**-PO_4 (*red*), *Ec*PanK-AMPPNP (*magenta*, PDB code 1ESN), *Ec*PanK-Pan-ADP (*blue*, PDB code 1SQ5), and *Cb*PanK-ADP (*yellow*, PDB code 3TQC) showing the open and closed forms of the adenosine lid.

Attempts to obtain binary complexes of *Mt*PanK with ATP or ternary complexes with inhibitory compounds and ATP, whether by co-crystallization or soaking in conditions for the orthorhombic space group, were unsuccessful. Non-hydrolyzable ATP analogues, adenosine, adenosine ribose, or ADP were also used in place of ATP but without success. Although some crystals were obtained and diffraction data were collected, the resolution and data quality did not allow modeling of the entities seen in the active site. The high phosphate concentration required for crystallization in this space group, resulting in a phosphate occupying the P-loop or potentially close contacts between our inhibitors and the γ-phosphate of ATP, may account for our inability to crystallize *Mt*PanK with bound ATP analogues.

IC_{50}, Minimum Inhibitory Concentration, and Thermal Stability Measurements—Detailed results for related inhibitory compounds of the classes presented here have been described (17). The loss of inhibition of the triazole compounds when the assay was run in excess of ATP (Table 2) indicates that these compounds compete with ATP. This is supported by the thermal stability measurements of these compounds where a decrease in the thermal shift is observed when the measurements are performed at higher ATP concentrations (Table 2). The biaryl compound **2a** shows comparable levels of inhibition at low and high ATP concentrations, suggesting that this class of compounds is non-competitive with respect to ATP. The thermal stability measurements for this compound show an increase in thermal shift in the presence of ATP, also indicative of a non-competitive mode of inhibition. Unfortunately, inhibition in the presence of ATP and thermal stability measurements were not available for compound **2b**. None of the compounds described here inhibited growth of *Mt* in the whole cell assay at their respective maximum concentration tested (Table 2).

DISCUSSION

We have determined the first enzyme-inhibitor complex structures of a type I PanK enzyme. The structures show that the two classes of inhibitory compounds, triazoles and biaryls, bind in roughly the same position, overlapping with binding sites for the substrate pantothenate and product phosphopantothenate.

The six triazole complexes provide 12 views of how this class of inhibitor interacts with *Mt*PanK. The inhibitors share a common binding site with the same overall U-shaped structure and share many equivalent interactions with the enzyme and structurally conserved water molecules. In particular, the hydrogen bonding network of the triazole nitrogens with residues Tyr-235 and Asn-277 is a feature of this class of inhibitor. Modulation in IC_{50} values has been achieved by the introduction of halogen atoms and/or groups, by removal of the ether-linked oxygen, and by an extension from the central triazole ring. The benefits of introducing fluorine atoms on small molecule scaffolds is well documented, and structural data have been used to clarify the nature of fluorine-protein interactions. It has been suggested that C-F dipolar and multipolar interactions with protein side chain and main chain atoms can benefit the energetics of inhibitor binding (30). Favorable interactions with backbone and side chain amides as well as the guanidinium group of arginine residues appear to be common occurrences. The top four, most active triazoles (**1a**, **1c**, **1d**, and **1e**) contain a trifluoromethyl substitution that is positioned close to the imidazole ring of His-179, with closest contacts in the range 3.3–3.7 Å. The trifluoromethyl group points toward the edge of the second phenyl ring of each inhibitor to form other, potentially stabilizing multipolar interactions. The combined effects may be sufficient to explain the 10-fold increase in IC_{50} values that are observed for **1b** and **1f** where the trifluoromethyl group has been substituted. In seven of the eight triazoles, the second phenyl ring is also fluorinated at the para-position. In these structures, we observe an interaction with the guanidinium group of Arg-238, but the removal of the fluorine atom does not reduce the activity of **1d**. The replacement of the *para*-fluorophenyl ring by an *ortho*-methylphenyl ring in **1d** results in a structural rearrangement such that the ring to ring centers are closer in **1d**

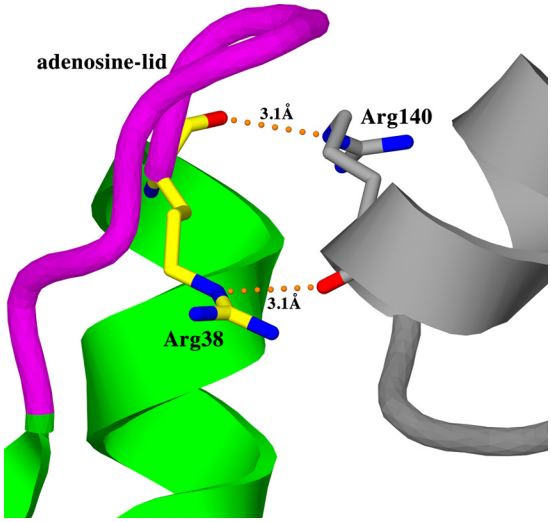

FIGURE 7. **Crystal contacts between the adenosine lid (*magenta*) of *Mt*PanK-1a (*green*) in the orthorhombic space group and a symmetry-related molecule (*gray*).** Shown are interactions between Arg-38 in the adenosine lid (*yellow* carbons) and Arg-140 in helix α7 of the symmetry-related molecule (*gray* carbons).

by 0.3 Å. This may benefit the interactions with the trifluoromethyl group sufficiently so that there is little change in the IC_{50} compared with **1a**, for example.

IC_{50} values for the biaryl compounds are comparable with those for the triazole compounds, with **2a** having the lowest IC_{50} (Table 2). The approximate 5-fold increase in IC_{50} for compound **2b** can be due to the lack of a hydrogen bond to the guanido group of Arg-238 and the apparent weakening of the hydrogen bond to Tyr-182, which is absent in the B molecule due to side chain rotation.

Increasing the ATP concentration in the biochemical assay resulted in a large increase of the IC_{50} for all triazole compounds (Table 2). This suggests that these compounds exhibit a competitive mode of binding with respect to ATP. The same increase in ATP concentration does not affect the biaryl compounds (Table 2), suggesting that these compounds exhibit a non-competitive mode of binding. This observation is also supported by the thermal shift measurements where addition of ATP resulted in a decrease in T_m in the presence of triazole compounds and an increase with the biaryl compounds (Table 2). The superimposed ATP analogue complexes of the *Mt* and *Ec* enzymes (Fig. 5*c*) provide a likely explanation. In all triazole complexes, an electronegative fluorine or chlorine is in close contact with the γ-phosphate oxygen of an ATP analogue. The repulsive electrostatic force between these atoms results in the competitive binding mode of these compounds. In the biaryl complexes, these interactions are absent, making it possible for the non-competitive binding mode observed for this class of compounds.

In all previously reported *Mt*PanK structures, solved in what has been described as crystal form I or II of the trigonal space group, the adenosine lid is in a closed conformation. The *Mt*PanK-**1a** complex, crystallized in crystal form II of the trigonal space group, also exhibits a closed conformation of the adenosine lid. An examination of the crystal contacts in this crystal form reveals that the adenosine lid is in close contact with helix α7 of a symmetry-related molecule (Fig. 7). In particular, the guanidinium group of residue Arg-38 in the adenosine lid forms a hydrogen bond to the carbonyl oxygen of residue Arg-140 in helix α7 of the symmetry-related molecule. These crystal packing interactions are present in all *Mt*PanK structures solved in crystal form II but not in the two structures solved in crystal form I (*Mt*PanK-CoA, PDB codes 2GES and 2GET). Crystal packing interactions with the adenosine lid are also absent in our structures solved in the orthorhombic space group, where the adenosine lid adopts an open conformation. In contrast, the complex structures with nucleoside cofactors were crystallized in crystal form II of the trigonal space group, where the adenosine lid assumes a closed conformation. In these structures, the adenosine or guanosine moieties occupy roughly the same binding site as the adenosine moiety of CoA instead of binding in the adenosine binding site (Fig. 5, *b* and *c*). Crystal contacts with the adenosine lid in these structures may be responsible for keeping the adenosine lid in a closed conformation, forcing the nucleoside cofactors to adopt an alternative binding mode. To date, no crystal structure of a nucleoside-bound enzyme has been solved in the orthorhombic space group or crystal form I of the trigonal space group. However, the conserved nature of the adenosine binding site and the ability of *Mt*PanK to adopt both open and closed forms of the adenosine-lid suggest that the same mode of nucleoside binding as seen in the *Ec* and *Cb* enzymes is biologically relevant.

Even though the compounds described in this study were inactive against *Mt* in the whole cell assay, they are potent inhibitors of *Mt*PanK. The structural information from this study provides us with tools for structure-based optimization of these compounds and to design novel inhibitors that are active against this target in other pathogens.

Acknowledgments—We acknowledge the work of Kishore B. K. Reddy, Subramanyam J. Tantry, Sudhir Landge, Aishwarya Sundaram, Jagannathan Alagurajan, Harini Iyer, Jyothi Bhat, and N. Radha for compound synthesis and technical support.

REFERENCES

1. Jackowski, S., and Rock, C. O. (1981) Regulation of coenzyme A biosynthesis. *J. Bacteriol.* **148,** 926–932
2. Dunn, S. D., and Snell, E. E. (1979) Isolation of temperature-sensitive pantothenate kinase mutants of *Salmonella typhimurium* and mapping of the coaA gene. *J. Bacteriol.* **140,** 805–808
3. Vallari, D. S., Jackowski, S., and Rock, C. O. (1987) Regulation of pantothenate kinase by coenzyme A and its thioesters. *J. Biol. Chem.* **262,** 2468–2471
4. Song, W. J., and Jackowski, S. (1994) Kinetics and regulation of pantothenate kinase from *Escherichia coli*. *J. Biol. Chem.* **269,** 27051–27058
5. Yun, M., Park, C. G., Kim, J. Y., Rock, C. O., Jackowski, S., and Park, H. W. (2000) Structural basis for the feedback regulation of *Escherichia coli* pantothenate kinase by coenzyme A. *J. Biol. Chem.* **275,** 28093–28099
6. Zhou, B., Westaway, S. K., Levinson, B., Johnson, M. A., Gitschier, J., and Hayflick, S. J. (2001) A novel pantothenate kinase gene (PANK2) is defective in Hallervorden-Spatz syndrome. *Nat. Genet.* **28,** 345–349
7. Rock, C. O., Karim, M. A., Zhang, Y. M., and Jackowski, S. (2002) The murine pantothenate kinase (Pank1) gene encodes two differentially regulated pantothenate kinase isozymes. *Gene* **291,** 35–43
8. Leonardi, R., Chohnan, S., Zhang, Y. M., Virga, K. G., Lee, R. E., Rock, C. O., and Jackowski, S. (2005) A pantothenate kinase from *Staphylococcus*

aureus refractory to feedback regulation by coenzyme A. *J. Biol. Chem.* **280,** 3314–3322
9. Yang, K., Eyobo, Y., Brand, L. A., Martynowski, D., Tomchick, D., Strauss, E., and Zhang, H. (2006) Crystal structure of a type III pantothenate kinase: insight into the mechanism of an essential coenzyme A biosynthetic enzyme universally distributed in bacteria. *J. Bacteriol.* **188,** 5532–5540
10. Brand, L. A., and Strauss, E. (2005) Characterization of a new pantothenate kinase isoform from *Helicobacter pylori*. *J. Biol. Chem.* **280,** 20185–20188
11. Awasthy, D., Ambady, A., Bhat, J., Sheikh, G., Ravishankar, S., Subbulakshmi, V., Mukherjee, K., Sambandamurthy, V., and Sharma, U. (2010) Essentiality and functional analysis of type I and type III pantothenate kinases of *Mycobacterium tuberculosis*. *Microbiology* **156,** 2691–2701
12. Walker, J. E., Saraste, M., Runswick, M. J., and Gay, N. J. (1982) Distantly related sequences in the α- and β-subunits of ATP synthase, myosin, kinases and other ATP-requiring enzymes and a common nucleotide binding fold. *EMBO J.* **1,** 945–951
13. Das, S., Kumar, P., Bhor, V., Surolia, A., and Vijayan, M. (2006) Invariance and variability in bacterial PanK: a study based on the crystal structure of *Mycobacterium tuberculosis* PanK. *Acta Crystallogr. D Biol. Crystallogr.* **62,** 628–638
14. Chetnani, B., Das, S., Kumar, P., Surolia, A., and Vijayan, M. (2009) *Mycobacterium tuberculosis* pantothenate kinase: possible changes in location of ligands during enzyme action. *Acta Crystallogr. D Biol. Crystallogr.* **65,** 312–325
15. Chetnani, B., Kumar, P., Surolia, A., and Vijayan, M. (2010) *M. tuberculosis* pantothenate kinase: dual substrate specificity and unusual changes in ligand locations. *J. Mol. Biol.* **400,** 171–185
16. Chetnani, B., Kumar, P., Abhinav, K. V., Chhibber, M., Surolia, A., and Vijayan, M. (2011) Location and conformation of pantothenate and its derivatives in *Mycobacterium tuberculosis* pantothenate kinase: insights into enzyme action. *Acta Crystallogr. D Biol. Crystallogr.* **67,** 774–783
17. Venkatraman, J., Bhat, J., Solapure, S. M., Sandesh, J., Sarkar, D., Aishwarya, S., Mukherjee, K., Datta, S., Malolanarasimhan, K., Bandodkar, B., and Das, K. S. (2012) Screening, identification, and characterization of mechanistically diverse inhibitors of the *Mycobacterium tuberculosis* enzyme, pantothenate kinase (CoaA). *J. Biomol. Screen.* **17,** 293–302
18. Franzblau, S. G., Witzig, R. S., McLaughlin, J. C., Torres, P., Madico, G., Hernandez, A., Degnan, M. T., Cook, M. B., Quenzer, V. K., Ferguson, R. M., and Gilman, R. H. (1998) Rapid, low-technology MIC determination with clinical *Mycobacterium tuberculosis* isolates by using the microplate Alamar Blue assay. *J. Clin. Microbiol.* **36,** 362–366
19. Leslie, A. G. (2006) The integration of macromolecular diffraction data. *Acta Crystallogr. D Biol. Crystallogr.* **62,** 48–57
20. Evans, P. (2006) Scaling and assessment of data quality. *Acta Crystallogr. D Biol. Crystallogr.* **62,** 72–82
21. Winn, M. D., Ballard, C. C., Cowtan, K. D., Dodson, E. J., Emsley, P., Evans, P. R., Keegan, R. M., Krissinel, E. B., Leslie, A. G., McCoy, A., McNicholas, S. J., Murshudov, G. N., Pannu, N. S., Potterton, E. A., Powell, H. R., Read, R. J., Vagin, A., and Wilson, K. S. (2011) Overview of the CCP4 suite and current developments. *Acta Crystallogr. D Biol. Crystallogr.* **67,** 235–242
22. Murshudov, G. N., Skubák, P., Lebedev, A. A., Pannu, N. S., Steiner, R. A., Nicholls, R. A., Winn, M. D., Long, F., and Vagin, A. A. (2011) REFMAC5 for the refinement of macromolecular crystal structures. *Acta Crystallogr. D Biol. Crystallogr.* **67,** 355–367
23. McCoy, A. J., Grosse-Kunstleve, R. W., Adams, P. D., Winn, M. D., Storoni, L. C., and Read, R. J. (2007) Phaser crystallographic software. *J. Appl. Crystallogr.* **40,** 658–674
24. Jones, T. A., Zou, J. Y., Cowan, S. W., and Kjeldgaard, M. (1991) Improved methods for building protein models in electron density maps and the location of errors in these models. *Acta Crystallogr. A* **47 (Pt 2),** 110–119
25. Harris, M., and Jones, T. A. (2001) Molray–a web interface between O and the POV-Ray ray tracer. *Acta Crystallogr. D Biol. Crystallogr.* **57,** 1201–1203
26. Kleywegt, G. J., and Jones, T. A. (1997) Detecting folding motifs and similarities in protein structures. *Methods Enzymol.* **277,** 525–545
27. Larkin, M. A., Blackshields, G., Brown, N. P., Chenna, R., McGettigan, P. A., McWilliam, H., Valentin, F., Wallace, I. M., Wilm, A., Lopez, R., Thompson, J. D., Gibson, T. J., and Higgins, D. G. (2007) Clustal W and Clustal X version 2.0. *Bioinformatics* **23,** 2947–2948
28. Bond, C. S., and Schüttelkopf, A. W. (2009) ALINE: a WYSIWYG protein-sequence alignment editor for publication-quality alignments. *Acta Crystallogr. D Biol. Crystallogr.* **65,** 510–512
29. Ivey, R. A., Zhang, Y. M., Virga, K. G., Hevener, K., Lee, R. E., Rock, C. O., Jackowski, S., and Park, H. W. (2004) The structure of the pantothenate kinase.ADP.pantothenate ternary complex reveals the relationship between the binding sites for substrate, allosteric regulator, and antimetabolites. *J. Biol. Chem.* **279,** 35622–35629
30. Müller, K., Faeh, C., and Diederich, F. (2007) Fluorine in pharmaceuticals: looking beyond intuition. *Science* **317,** 1881–1886
31. Matthews, B. W. (1968) Solvent content of protein crystals. *J. Mol. Biol.* **33,** 491–497
32. Kleywegt, G. J., and Jones, T. A. (1996) Phi/psi-chology: Ramachandran revisited. *Structure* **4,** 1395–1400
33. Engh, R. A., and Huber, R. (1991) Accurate bond and angle parameters for X-ray protein structure refinement. *Acta Crystallogr. A* **47,** 392–400
34. Read, R. J. (1986) Improved Fourier coefficients for maps using phases from partial structures with errors. *Acta Crystallogr. D Biol. Crystallogr.* **42,** 140–149